Detectability of active triangulation range finder: a solar irradiance approach

Huizhe Liu,[1,*] Jason Gao,[2] Viet Phuong Bui,[1] Zhengtong Liu,[1] Kenneth Eng Kian Lee,[3] Li-Shiuan Peh,[2] and Ching Eng Png[1]

[1]*Electronics and Photonics Department, Institute of High Performance Computing, Agency for Science, Technology and Research (A*STAR), 138632, Singapore*
[2]*Department of Electrical Engineering and Computer Science, Massachusetts Institute of Technology, USA*
[3]*Low Energy Electronic Systems IRG, Singapore-MIT Alliance for Research and Technology, Singapore*
[*]*liuh@ihpc.a-star.edu.sg*

Abstract: Active triangulation range finders are widely used in a variety of applications such as robotics and assistive technologies. The power of the laser source should be carefully selected in order to satisfy detectability and still remain eye-safe. In this paper, we present a systematic approach to assess the detectability of an active triangulation range finder in an outdoor environment. For the first time, we accurately quantify the background noise of a laser system due to solar irradiance by coupling the Perez all-weather sky model and ray tracing techniques. The model is validated with measurements with a modeling error of less than 14.0%. Being highly generic and sufficiently flexible, the proposed model serves as a guide to define a laser system for any geographical location and microclimate.

OCIS codes: (280.3400) Laser range finder; (140.3360) Laser safety and eye protection; (290.4210) Multiple scattering.

References and links

1. L. Matthies, T. Balch, and B. Wilcox, "Fast optical hazard detection for planetary rovers using multiple spot laser triangulation," in *Proceedings of IEEE International Conference on Robotics and Automation (ICRA)* (IEEE, 1997), pp. 859–866.
2. C. Mertz, J. Kozar, J. R. Miller, and C. Thorpe, "Eye-safe laser line striper for outside use," in *Proceedings of IEEE Intelligent Vehicle Symposium* (IV, 2002), pp. 507–512.
3. M. Levoy, K. Pulli, B. Curless, S. Rusinkiewicz, D. Koller, L. Pereira, M. Ginzton, S. Anderson, J. Davis, J. Ginsberg, J. Shade, and D. Fulk, "The digital Michelangelo project: 3D scanning of large statues," in *Proceedings of the 27th Annual Conference on Computer Graphics and Interactive Techniques* (SIGGRAPH, 2000), pp. 131–144.
4. D. Ilstrup and R. Manduchi, "Active triangulation in the outdoors: a photometric analysis," in *Fifth International Symposium on 3D Data Processing, Visualization and Transmission* (3DPVT, 2010).
5. J. H. Gao and L.-S. Peh, "A smartphone-based laser distance sensor for outdoor environments," in *2016 IEEE International Conference on Robotics and Automation* (ICRA, 2016), pp. 2922–2929.
6. D. Yuan and R. Manduchi, "A tool for range sensing and environment discovery for the blind," in *Proceedings of the IEEE Conference on Computer Vision and Pattern Recognition Workshop (CVPRW)* (IEEE, 2004), pp. 39.
7. P. de la Hamette, M. von Waldkirch, and G. Tröster, "Laser triangulation as a means of robust visual input for wearable computers," in *Proceedings of the 4th International Symposium on Wearable Computers (ISWC)* (2004), pp. 18–20.
8. E. Guizzo, "How Google's self-driving car works," *IEEE Spectrum Online* **18** (2011).
9. ANSI standard Z136.1–2000, American national standard for the safe use of lasers, Laser Institute of America.
10. K. P. Lam, A. Mahdavi, M. B. Ullah, E. Ng, and V. Pal, "Evaluation of six sky luminance prediction models using measured data from Singapore," Light. Res. Technol. **31**(1), 13–17 (1999).
11. A. Gruen, X. Huang, R. Qin, T. Du, W. Fang, J. Boavida, and A. Oliveira, "W, Fang, J. Boavida, A. Oliveira, D. J. Thevenard and A. P. Brunger, "Joint processing of UAV imagery and terrestrial mobile mapping system data for very high resolution city modeling," *ISPRS* -," Int. Arch. Photogramm. Remote Sens. Spat. Inf. Sci **XL-1**(W2), 175–182 (2013).
12. Radiance software, (http://radsite.lbl.gov/) developed by the Lawrence Berkeley National Laboratory.

#264656 Received 6 May 2016; revised 19 Jun 2016; accepted 19 Jun 2016; published 22 Jun 2016

1. Introduction

Laser range finders are widely used in robotics applications for distance detection [1]. They have also been applied to autonomous vehicles [2,8], cultural heritage digitization [3], assistive technology [6], and human computer interaction [7]. Laser range finders mainly operate on one of the two techniques: time-of-flight [8] and triangulation [1–7]. Time-of-flight range finders tend to have higher cost due to the high precision equipment needed to register the returned signal. The triangulation range finders are of low-cost, low-power and high portability for short-medium range applications, and are of interest to this paper.

For active triangulation range finders, various sources of structured laser light exist, such as spot [6], line striper [1–5] or laser array [7]. Unlike the spot laser that measures a point from each camera frame, the laser line striper measures distances to multiple points along an illuminated profile line. The laser line striper, being more efficient than the spot laser and being simpler in structure than the laser array, is the most popular choice for 3D scanning of the environment and is chosen for illustrative purpose in this paper. The main challenge with laser line striper is its detectability as its power spreads over a fan angle making it vulnerable to the background noise.

Laser detectability is subject to the background noise which mainly comes from solar irradiance in an outdoor environment. Existing work on triangulation range finders estimate solar irradiance using tables for solar spectral irradiance [4,7]. Such practice has obvious limitations. Firstly, surfaces are treated as 37°-tilted and south-facing as a representation of the average latitude of 48 contiguous United States, which is an over-simplification of the actual scene. Secondly, only direct solar irradiance is considered. However, the diffuse component of solar irradiance does play an important role when the sky has considerable cloud cover which is commonly observed in the tropics or in a built-up environment where multiple scattering is inevitable. For the first time, we accurately quantify both the direct and diffuse solar irradiance for assessing the laser detectability. In Section 2, we present a generic model to gauge the laser detectability, and briefly discuss its applicability for source selection. We validate the model with measurements in Section 3 and conclude the paper in Section 4.

2. Methodology

2.1 System overview

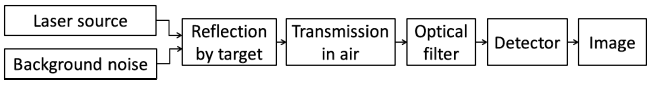

Fig. 1. Block diagram of an active triangulation range finder.

As shown in Fig. 1, the major components of the overall laser system are: the laser source, the background noise, the reflection by target, the transmission in air, filtering, and the camera's imager as detector. The output is an image, from which the range information of laser-illuminated pixels can be extracted via the triangulation technique. The modeling of individual components of the overall system is elaborated in subsequent subsections.

2.2 Detectability model

As illustrated in Fig. 2, we use a laser line striper as an example, which has output power P_{lsr}, beam divergence γ, fan angle β, and beam diameter d. Its wavefront at range R can be characterized by an arc length $D_1 = R\beta + d \approx R\beta$ (under the assumption $R\beta >> d$) and a narrow width $D_2 = R\gamma + d$. The laser striper subtends a solid angle given by $\Omega(R) = D_1 D_2 / R^2 \approx \beta(\gamma + d/R)$. The power of laser striper is assumed to be uniformly distributed through the solid angle. Hence, the laser irradiance on a target surface at range R can be shown to be [4]

#264656 Received 6 May 2016; revised 19 Jun 2016; accepted 19 Jun 2016; published 22 Jun 2016

$$I_{\text{lsr}} = P_{\text{lsr}} \cos\theta_{\text{lsr}} \Big/ \left[\Omega(R) R^2\right], \tag{1}$$

where θ_{lsr} is the angle between the surface normal and the incident direction of the laser beam.

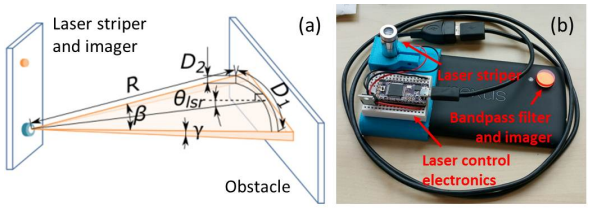

Fig. 2. (a) Schematic view of the overall set-up, (b) photo of a smartphone with laser striper [5].

The solar irradiance I_{sol} is the main source of background noise that affects detectability in an outdoor environment. In previous work, only the direct component of the solar irradiance is considered. For more accurate description, we take into account of the both the direct and diffuse component of solar irradiance. We make use of a sky model to describe the direction and intensity of the natural light sources and employ ray tracing techniques to address the multiple scatterings in the scene. As shown in Fig. 3, the inputs to the ray tracing engine are the sky model, the scene geometry and probes on target. The output is I_{sol} at the probes.

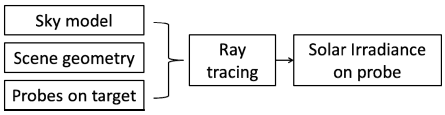

Fig. 3. Flowchart of background noise model in an outdoor environment.

The total irradiance at any point on a target surface is the summation of the laser and solar irradiance as given by $I_{\text{tot}} = I_{\text{lsr}} + I_{\text{sol}}$. Once the laser beam and the solar radiation hit the target surface, they are reflected and a fraction reaches the detector. Lambertian reflectance model is most commonly used to describe the reflectance event on target surface [1], by assuming the surface reflects the light equally in all directions with outgoing radiance $L = \rho I_{tot} / \pi$ where ρ denotes the diffuse reflectance of the surface material. Admittedly, most of the diffusely-reflecting materials also have some degree of specular reflectance and surface roughness, which should be taken into account for more accurate material modeling. Transmission in air is lossless in general, unless the weather is hazy or misty.

A bandpass filter with response function $H(\lambda)$ is placed in front of the camera to cut down background noise, where λ is the wavelength. The irradiance falling on a camera pixel can be expressed as [4] $I_{pix} = C(\alpha)\int_{-\infty}^{\infty} L(\lambda) H(\lambda)\, d\lambda$, where $C(\alpha) = (\pi/4)(D/f)^2 A(\alpha)$. $L(\lambda)$ is the radiance from the target surface, D is the lens diameter, f is the focal length, and $A(\alpha)$ accounts for the effect of the off-axis angle α which is an angle between a ray from the pixel through the center of the lens and the principle axis [4]. For a filter with passband λ_{p}, its spectral response for the background radiation can be represented by an effective response $H(\lambda_{\text{p}}) = r_{\lambda\text{p}}\, t_{\lambda\text{p}}$, where $r_{\lambda\text{p}} = \int_{\lambda\text{p}} I_{\text{spec}}\, d\lambda \,/\, \int_{\lambda\text{full}} I_{\text{spec}}\, d\lambda$ is the ratio of the summed solar spectral irradiance I_{spec} within λ_{p} to the sum in the full solar spectra λ_{full}; $t_{\lambda\text{p}}$ is the effective transmittance within λ_{p}. The filter response at operating wavelength λ_0 of the laser is denoted by $H(\lambda_0) = t_{\lambda 0}$. The irradiance on a pixel can be rewritten as

$$I_{\text{pix}} = (\rho/\pi) C(\alpha)\left(I_{\text{lsr}} t_{\lambda_0} + I_{\text{sol}} r_{\lambda_{\text{p}}} t_{\lambda_{\text{p}}}\right). \tag{2}$$

For raw images, the pixel values are directly proportional to the irradiance on a pixel $M_{\text{tot}} = \Gamma I_{\text{pix}}$ where Γ represents the camera exposure setting [4].

We define a metric, the brightness ratio B, to gauge the laser detectability, given by

#264656 Received 6 May 2016; revised 19 Jun 2016; accepted 19 Jun 2016; published 22 Jun 2016

$$B = I_{\text{pix,tot}} \big/ I_{\text{pix,bg}}\,, \tag{3}$$

where $I_{\text{pix, tot}}$ ($I_{\text{pix,bg}}$) is the irradiance value of a pixel with (without) laser return.

By substituting Eq. (2) into Eq. (3), we have

$$B = \frac{I_{\text{pix,tot}}}{I_{\text{pix,bg}}} = \frac{\rho_{\text{lsr}}}{\rho_{\text{bg}}} \frac{C\left(\alpha_{\text{lsr}}\right)}{C\left(\alpha_{\text{bg}}\right)} \frac{I_{\text{lsr}} t_{\lambda_0} + I_{\text{sol}} r_{\lambda_p} t_{\lambda_p}}{I_{\text{sol}} r_{\lambda_p} t_{\lambda_p}}, \tag{4}$$

where ρ_{lsr} and ρ_{bg} are the surface albedo in the scene corresponding to two pixels, one with laser return and one without; α_{lsr} and α_{bg} are the respective off-axis angles of the two pixels. As a rule of thumb, $B > 1$ should always hold to ensure that the pixels with laser return are always brighter than the background pixels for ease of detection [1]. While designing the laser system, the range of albedo in the scene should be carefully surveyed in order to obtain B in the worst case scenario, with ρ_{lsr} (ρ_{bg}) equals the lowest (highest) albedo in the scene.

2.3 Eye safety

The choice of wavelength of the laser source should be guided by eye safety considerations. Visible lasers are subject to relatively higher background noise and ultraviolet lasers are known to be hazardous to the retina. In comparison, infrared lasers are the most suitable for outdoor applications. It should be cautioned that the wavelength should not go too far into the infrared region, as the sensitivity of the CMOS image sensor of the camera may decline.

The maximal source power is confined by eye-safety considerations. According to the American National Standards Institution (ANSI) standard [9], the maximum permissible energy (MPE) in J/cm^2 for continuous wave (CW) laser of wavelength λ_0 between 700nm and 1050nm and exposure duration t between 18×10^{-6}s and 10s is denoted as MPE = $1.8C_{\text{A}}t^{0.75} \times 10^{-3}$ where $C_A = 10^{2(\lambda 0\text{-}700)}$. The maximum permissible energy per exposure is given by E = MPE•$A(\beta R/D_2)$ where $A = 0.385\text{cm}^2$ is the area of the pupil, R is the range, and D_2 is the thickness of laser line striper at range R. As such, the upper bound of the source power is

$$P_{\text{lsr,max}} = R_{\text{min}} \cdot MPE \cdot A\beta \big/ \left(tD_2\right). \tag{5}$$

2.4 Model applicability

The proposed detectability model enables quick and fairly accurate estimation of the source power at the design stage. By setting B > 1 and substituting Eq. (1) to Eq. (4), the lower bound of the source power can be expressed as

$$P_{\text{lsr,min}} = \frac{\left[\rho_{bg} C\left(\alpha_{bg}\right) - \rho_{\text{lsr}} C\left(\alpha_{lsr}\right)\right] I_{\text{sol}} r_{\lambda_p} t_{\lambda_p}}{\cos\theta_{\text{lsr}} \rho_{\text{lsr}} C\left(\alpha_{lsr}\right) t_{\lambda_0}} \Omega\left(R\right) R^2. \tag{6}$$

For instance, with reference to Eqs. (5) and (6), a laser striper with $P_{\text{lsr}} = 80$mW is chosen for model validation, given $R_{\text{min}} = 50$cm, $D_2 = 7$mm and the scenario described in Section 3.

The model is highly generic and can be applied to different scenarios, by adjusting the corresponding components of the model. For instance, to apply to a different scene, one can simply input appropriate local geographical and weather data into the sky model, and adopt the geometrical model of the actual scene for the ray tracing process. For an indoor environment, the sky model should be replaced by indoor light sources. When a different type of laser is used, i.e. spot laser, appropriate laser model should be adopted. If pulsed laser is used, corresponding eye-safety requirement for pulsed laser should be checked.

#264656 Received 6 May 2016; revised 19 Jun 2016; accepted 19 Jun 2016; published 22 Jun 2016

3. Model validation

3.1 Measurement set-up

The images of the laser striper were collected using a modified Nexus 5 smartphone shown in Fig. 2(b) at specific distances, i.e. 0.5m, 1.0m, and 1.5m, on two north-facing walls shown in Fig. 4 at 12:30 and 14:30 on 24 June in Singapore. The specifications of the laser striper are λ_0 = 780nm, P_{lsr} = 80mW, β = 1.57rad, d = 6.8mm, and γ = 2mrad. The infrared cut-off filter within the camera module was removed to enable infrared light to be collected on the CMOS image sensor. In front of the camera lens, we also placed an external optical bandpass filter with λ_0 = 780nm and bandwidth 20 ± 4nm. The pixel values in the raw images (*.dng*) are normalized to facilitate visualization. The normalized and cropped images are presented in Figs. 5 and 6. In actual application, more complex image processing techniques should be applied to address noises from laser speckling, camera noise, and so on [5].

Fig. 4. Overview photo of measurement location with target surfaces circled.

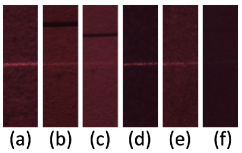

Fig. 5. Normalized and cropped images at 12:30 on wall 1 at (a) 0.5m, (b) 1.0m, (c) 1.5m; on wall 2 at (d) 0.5m, (e) 1.0m, and (f) 1.5m.

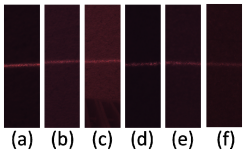

Fig. 6. Normalized and cropped images at 14:30 on wall 1 at (a) 0.5m, (b) 1.0m, (c) 1.5m; on wall 2 at (d) 0.5m, (e) 1.0m, and (f) 1.5m.

3.2 Simulation set-up

The solar irradiance distribution in the scene is modeled with reference to Fig. 3. The Perez all-weather sky model is adopted, which is known to be one of the most suitable sky models for Singapore [10]. The scene geometry was constructed by Gruen et *al*. using images from unmanned aerial vehicles, point cloud data from mobile mapping system and terrestrial images [11]. As shown in Fig. 4, wall 1 and 2 are respectively made from sandstone and graphite tiles with ρ_{wall} = 0.35, and the ground comprises of grass and concrete with ρ_{ground} = 0.2. A probe is positioned on each target wall, to mark where the laser beam is shone. The solar irradiance I_{sol} at the probes and in the scene is computed using *Radiance* [12].

As described in Section 2, we employ the simplified model of a laser striper with specifications from Section 3.1, apply the Lambertian reflectance model, and assume the air is lossless. From the filter's datasheet, we have identified filter's transmittance to be $t_{\lambda 0}$ = 58.5% and $t_{\lambda p}$ = 39.5%. From the air mass 1.5 spectra, we obtain $r_{\lambda p}$ = 3.52%. The detector is the CMOS image sensor of a smartphone camera. The pixel with laser return and the background pixel are located in proximity with each other in the image center with $\alpha_{lsr} = \alpha_{bg} = 0^{\circ}$.

#264656 Received 6 May 2016; revised 19 Jun 2016; accepted 19 Jun 2016; published 22 Jun 2016

3.3 Result comparison

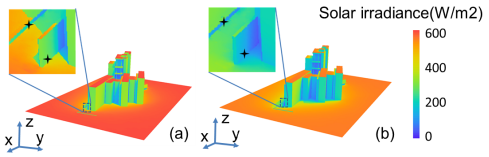

Fig. 7. Simulated solar irradiance distribution in the scene at (a) 12:30, and (b) 14:30 on 24 June. The insets show the zoom-in at the measurement sites (probes are marked by cross).

The solar irradiance distribution in the scene is shown in Fig. 7. Two probes are places at the measurement sites to obtain I_{sol} on the target surfaces. In Fig. 7(a), it is observed that at 12:30, the two probes are both exposed to the direct solar radiation, in agreement with Fig. 4. In Fig. 7(b), at 14:30, the two probes are in shade, in agreement with the measurement observation.

Next, we compute the brightness ratio B of two pixels, one with laser return and one without. From measurement data, $I_{pix,tot}$ is obtained by identifying the brightest pixel in each column in Figs. 5 and 6, and averaging across these columns; $I_{pix,bg}$ is obtained by averaging the background pixel values in an image. B is then computed for all configurations using Eq. (3). From simulation, B is computed using Eq. (4) with parameters specified in Section 3.2.

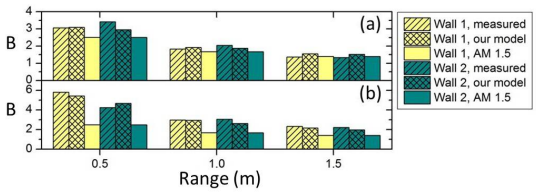

Fig. 8. Comparison of measured and simulated brightness ratios on wall 1 and wall 2 at (a) 12:30, and (b) 14:30 on 24 June.

As shown in Fig. 8, the measured and simulated B are in good agreement, whose differences are within 14.0% at 12:30 and 13.6% at 14:30. The results from a previous model, computed using a table of spectral response of the direct Sun (AM 1.5 spectrum), are also presented, with modeling error up to 26.7% at 12:30 and 56.9% at 14:30 [4,7]. In particular, at 14:30, the probe is in shade and receives background noise mainly from diffuse solar irradiance, which can be accurately captured by our model, and where the previous model that only accounts for direct Sun fails. The simulated and measured B is always larger than 1 signifying that the laser source with chosen power is detectable in all scenarios.

4. Conclusions

A highly generic model has been proposed to assess the detectability of an active triangulation range finder catered to the local scene and microclimate. In defining a laser system, the lower bound of source power is set by the proposed detectability model and the upper bound is set by the eye safety compliance. The detectability of a laser line striper with carefully chosen source power has been validated with measurements. The proposed methodology serves as a quick and fairly accurate guide for defining a laser system for detectable, eye-safe and energy-efficient operations in an outdoor environment.

Acknowledgments

We are grateful to Prof. Armin Gruen and Dr. Qin Rongjun from Singapore-ETH Center for assistance with the geometrical model. We are thankful to staff from DSO National Laboratories in Singapore for assistance in laser testing. We would like to thank Ms. Zheng Xuhui from CIAP Architects *Pte. Ltd.* for assistance in material identification in the scene.

#264656 Received 6 May 2016; revised 19 Jun 2016; accepted 19 Jun 2016; published 22 Jun 2016